EES Catalysis

MINIREVIEW

View Article Online
View Journal | View Issue

Cite this: *EES Catal.*, 2025, 3, 1030

Disassembling and reassembling perovskites for oxygen electrocatalysis

Gao Chen, *[a] Yubo Chen,[bc] Zezhou Lin,[d] Ting Chen,[e] Dongsheng Geng,[a] Yanping Zhu,*[e] Wei Wang[f] and Wei Zhou*[fg]

Perovskite oxides (ABO_3) are widely studied in oxygen electrocatalysis due to their simple synthesis routes, rich compositions, adjustable crystal/electronic structures, and high intrinsic activities. Despite these advantages, high calcination temperatures usually lead to agglomeration of perovskite materials, greatly reducing atomic utilization. Moreover, the different element features of A/B cations generally make easy enrichment of surface A-sites, and such surface deviation from the ideal structure would impede the precise illustration of structure–activity relationships for electrocatalysis. Up to now, various strategies have been developed to tackle the above issues, through which significant progress in both catalytic performance and underlying catalytic mechanisms has been achieved. Here we summarize those optimization methods as "disassembling and reassembling perovskites" and concisely review related studies and findings in terms of the fundamental understanding of approaches and the applications in oxygen electrocatalysis. Three typical methods, including physical, chemical, and electrochemical, are introduced with their effects on perovskite structures/catalytic mechanisms thoroughly discussed. Finally, four scientific issues regarding disassembling and reassembling perovskites are proposed for future studies. We aim to raise the community's awareness of this emerging approach and hope it could contribute to material design for applications beyond oxygen electrocatalysis.

Received 6th February 2025,
Accepted 8th May 2025

DOI: 10.1039/d5ey00036j

rsc.li/eescatalysis

Broader context

Perovskite oxides (ABO_3) have emerged as pivotal materials in oxygen electrocatalysis, underpinning critical energy conversion and storage technologies such as water electrolysis, fuel cells, and green electrochemical synthesis. Their compositional flexibility, tunable electronic structures, and high intrinsic activity position them as promising alternatives to noble metal catalysts. However, as-synthesized perovskites face inherent limitations, including low atomic utilization due to bulk particle formation at high synthesis temperatures and surface enrichment of inactive A-site cations, which obscure active B–O motifs and hinder precise structure–activity relationships. Addressing these challenges is vital to advancing sustainable energy systems and achieving global decarbonization goals. This work introduces 'disassembling and reassembling perovskites' as a transformative strategy to overcome these limitations. By leveraging physical, chemical, and electrochemical methods, the original perovskite structure is strategically broken down and reconfigured to enhance geometric and intrinsic activity, expose active sites, and clarify catalytic mechanisms. These approaches not only optimize oxygen evolution and reduction reactions but also unveil dynamic surface reconstruction phenomena and paracrystalline motifs, offering fresh insights into catalyst design. By bridging fundamental research with scalable engineering solutions, this work paves the way for next-generation materials that balance efficiency, stability, and cost-effectiveness in sustainable energy technologies.

[a] *Jiangsu Key Laboratory of New Energy Devices and Interface Science, School of Chemistry and Materials Science, Nanjing University of Information Science and Technology, Nanjing 210044, P. R. China. E-mail: gaochen@nuist.edu.cn*
[b] *Hydrogen Energy Institute, Zhejiang University, Hangzhou 310027, P. R. China*
[c] *Institute of Advanced Equipment, College of Energy Engineering, Zhejiang University, Hangzhou 310027, P. R. China*
[d] *Department of Applied Physics and Research Institute for Smart Energy, The Hong Kong Polytechnic University, Hong Kong, People's Republic of China*
[e] *College of Materials Science and Technology, Nanjing University of Aeronautics and Astronautics, Nanjing, People's Republic of China. E-mail: yanping.zhu@nuaa.edu.cn*
[f] *State Key Laboratory of Materials-Oriented Chemical Engineering, College of Chemical Engineering, Nanjing Tech University, Nanjing 211800, P. R. China. E-mail: zhouwei1982@njtech.edu.cn*
[g] *Suzhou Laboratory, Suzhou 215000, P. R. China*

1. Introduction

Oxygen electrocatalysis, encompassing the oxygen evolution reaction (OER) and oxygen reduction reaction (ORR), is fundamental to energy conversion and storage devices as well as green electrochemical synthesis with zero carbon emissions.[1–3] For example, the OER serves as the anode half-reaction in hydrogen production *via* water electrolysis, while the ORR functions as the cathode half-reaction in fuel cells and the electrochemical synthesis of hydrogen peroxide. Developing efficient and cost-effective oxygen electrocatalysts is crucial for enhancing catalytic conversion efficiency and reducing cost.[4,5]

Perovskite oxides (with the structural formula ABO_3) have served as pivotal materials in oxygen electrocatalysis for over four decades,[6] owing to their multifaceted merits such as straightforward synthesis methods, diverse compositions, tunable crystal and electronic structures, and high intrinsic activities.[7–9] Most perovskite oxides are synthesized by solid-phase and sol–gel processes, followed by calcination processes at high temperatures to form the perovskite phase. Some perovskites can be synthesized directly using hydrothermal methods, omitting further calcination. Approximately 90% of the elements in the periodic table can be incorporated into the perovskite structure. The substitution of A or B site elements allows precise tuning of crystalline and electronic structures. For example, by fine-tuning the constituent elements and their proportions, the $Ba_{0.5}Sr_{0.5}Co_{0.8}Fe_{0.2}O_{3-\delta}$ (BSCF) perovskite shows a unity filling in the e_g orbital, thus exhibiting the highest OER activity among a series of perovskites,[10] from which the use of perovskites as oxygen electrocatalysts has exploded, leading to significant breakthroughs in oxygen electrocatalysis. These include establishing e_g filling[10] and lattice oxygen mechanisms,[11,12] unveiling dynamic surface reconstruction,[13] defining stability numbers,[14] and finding paracrystalline motifs on reconstructed iridium perovskites.[15]

Despite these achievements, two main issues of perovskite oxides limit their further advancement. First, due to the high phase formation temperature (700–1200 °C), perovskite oxides usually exist as bulk particles, confining most active sites within the particles thus preventing their participation in surface oxygen electrocatalysis, resulting in low atom utilization.[16] Additionally, the intrinsic property difference between A and B cations makes easy enrichment of surface A-sites, leading to surface deviations from the ideal perovskite structure, posing challenges to the availability of the B site as well as the precise establishment of structure–activity relationship.[17,18]

In order to meet the higher requirements brought about by quick development of oxygen electrocatalysis, perovskite oxides have been tailored by various strategies to address the above mentioned issues, for which significant progress has been achieved. Here we unified those tailoring methods as "disassembling and reassembling perovskites"[19–21] and gave a comprehensive review of disassembling and reassembling perovskites for oxygen electrocatalysis. After defining disassembling and reassembling perovskites, advantages brought about by such tailoring are generalized. The materials discussed include traditional perovskites, layered perovskites, anti-perovskites, and non-oxide perovskites, spanning applications in acidic and alkaline OERs (from room temperature to 80 °C) as well as the alkaline ORR at room temperature. We classify those approaches into three categories: physical, chemical and electrochemical methods. The corresponding effects of each method on the perovskite structure, catalyst performance and the underlying catalytic mechanisms are discussed in detail, after which potential challenges and future directions regarding disassembling and reassembling perovskites for oxygen electrocatalysis are proposed.

Gao Chen

Gao Chen is a Professor in the School of Chemistry and Materials Science, Nanjing University of Information Science and Technology (NUIST). After obtaining his PhD degree from Nanjing Tech University, he received postdoc training at Nanyang Technology University and The Hong Kong Polytechnic University. His research interests cover designing high-efficiency electrocatalysts by disassembling and reassembling perovskites, as well as elucidating the fundamental connections between materials and reaction mechanisms in electrocatalysis.

Yanping Zhu

Yanping Zhu received her PhD in Chemical Engineering from Nanjing Tech University. From 2018 to 2023, she worked as a postdoctoral fellow at National Taiwan University and The Hong Kong Polytechnic University. In 2024, she joined the College of Materials Science and Technology at the Nanjing University of Aeronautics and Astronautics. Her research interests include developing advanced materials related to electrocatalysis and in situ methodologies toward various chemical reactions.

Wei Zhou

Wei Zhou received his PhD from Nanjing Tech University in 2009, focusing on the design and synthesis of high-performance cathode materials for solid oxide fuel cells (SOFCs). In 2010, he was awarded an Australian Postdoctoral Fellowship and joined the University of Queensland, where he was later promoted to a Research Fellow in 2013. In 2015, he returned to Nanjing Tech University as a Professor. His research interests encompass the development of advanced materials for SOFCs and electrocatalysts for oxygen reduction, water splitting, and CO_2 reduction reactions.

2. Fundamental understanding of disassembling and reassembling perovskites

The perovskite family adopts an ABO_3 structure, where A-site cations (Sr^{2+}, La^{3+}, *etc.*) occupy the voids within the framework of corner-sharing BO_6 octahedra, while the B-site transition metals (Co^{4+}, Fe^{3+}, *etc.*) occupy the octahedral center. Disassembling and reassembling perovskites involve breaking down the original structure of perovskites through specific methods and then recombining certain or all parts to form the target products. Whether the final product is perovskite or not depends on the method used. Experiencing such modification processes, the as-obtained materials usually have obvious advantages when participating in oxygen electrocatalysis including,

(i) Increasing geometrical activity by decreasing the size of the bulk perovskite to the nanoscale or the even atomic level. This is crucial for mitigating the adverse effects associated with the high phase-formation temperature of perovskites.

(ii) Enhancing intrinsic activity by manipulating component elements: removing inactive A-site elements while exposing active B–O octahedra with unusual local structure or abundant unsaturated coordination.

(iii) Precise illustration of structure–activity relationship by exposing specific lattice planes of perovskites enables more precise prediction of the relation between catalyst structure and catalytic performance.

3. Approaches used for disassembling and reassembling perovskites

Typically, the approaches utilized for disassembling and reassembling perovskites can be classified into three categories: physical, chemical, and electrochemical methods (Fig. 1).

(i) Physical methods: it generally refers to utilizing specific equipment to physically break the original perovskite structure and transform it into the desired states. The commonly used physical methods include pulsed laser deposition (PLD), magnetron sputtering, plasma etching, and ball milling.[22–24]

(ii) Chemical methods: through chemical reactions with perovskites using atmosphere or solution as medium, selective separation and rebuilding of perovskite components can be realized. The commonly used chemical approaches include exsolution, exfoliation, acid leaching, and chemical dissolution–deposition methods.[25–27]

(iii) Electrochemical methods: these methods are based on surface reconstruction of perovskites during electrocatalysis. Knowing that perovskites are rich in compositional elements, different components of perovskites exhibit different leach-deposition behaviors under the same pH and potential conditions, which could be predicted by the Pourbaix diagram. Desired disassembling and/or reassembling on perovskites can be realized by tuning composition, pH value of electrolyte and the applied potentials.[28]

4. Applications in oxygen electrocatalysis

According to previous studies, after disassembling and reassembling perovskites, the obtained catalyst materials are endowed with new properties, which in turn lead to satisfactory catalytic behaviors and help gain deep insights into the underlying mechanism of oxygen electrocatalysis. This section is organized by three typical categories of approaches for disassembling and reassembling perovskites. Features, advantages, corresponding effects and the applicability of each method are provided.

4.1. Physical methods and corresponding effects

4.1.1. Physical vapor deposition - making functional nanofilms. Physical vapor deposition (PVD) encompasses a family of vacuum deposition methods used to deposit thin films of various materials onto substrates (Fig. 2a). Operating at the atomic or molecular level, PVD processes vaporize the material

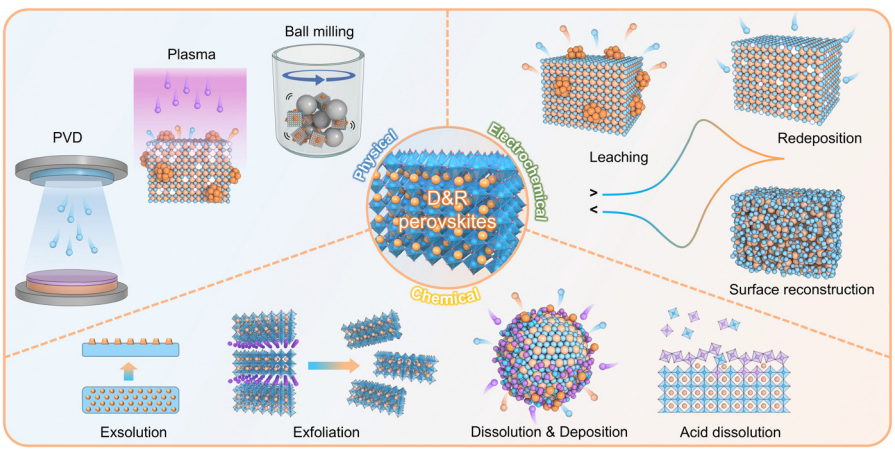

Fig. 1 Schematic illustration of the strategies for disassembling and reassembling perovskites. D&R perovskites: disassembling and reassembling perovskites.

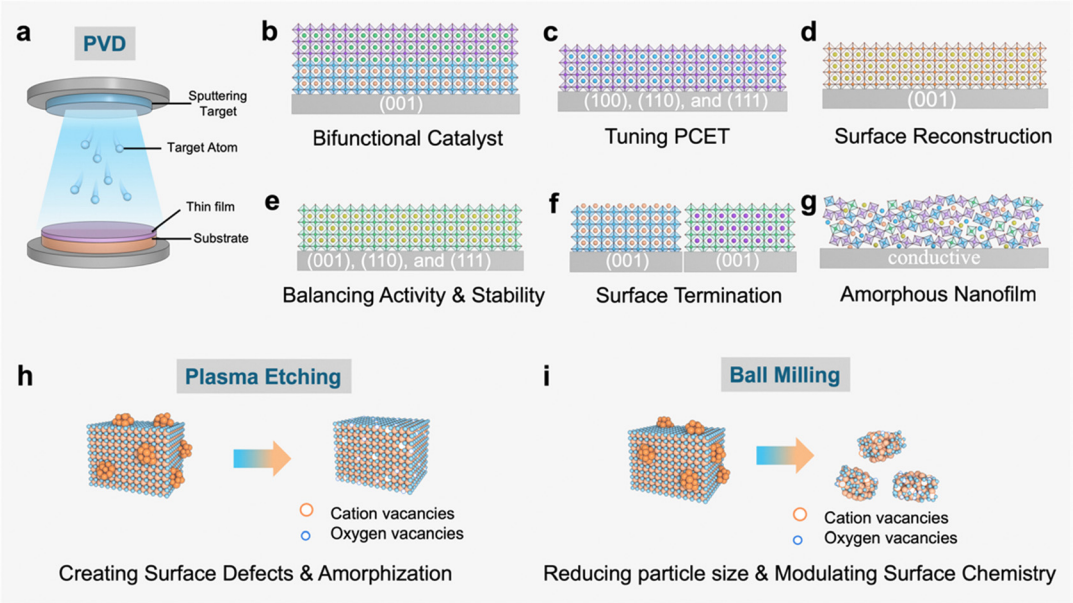

Fig. 2 Schematic illustration of physical strategies for disassembling and reassembling perovskites. (a) The physical vapor deposition (PVD) approach. (b)–(g) Examples of PVD approaches. (h) The plasma etching approach. (i) The ball milling approach. PCET: proton-coupled electron transfer.

from a solid or liquid source, transporting it in vacuum or low-pressure gas to the substrate, where it condenses. The resulting film properties depend on the specific process and materials used. PLD and magnetron sputtering are two common PVD techniques for disassembling and reassembling perovskites into functional nanofilms, yielding several benefits: (i) a nano-size perovskite thin film can be obtained, greatly improving the atom utilization of perovskites; (ii) single-crystal perovskites with specific orientations are obtained to accurately illustrate the structure–activity relationship; (iii) nanofilms exclude carbon additives, thus eliminating the current contribution of carbon to oxygen electrocatalysis; and (iv) breaking the long range ordered perovskite structure to form amorphous nanofilms. Here are some advanced examples of functional nanofilms synthesized *via* PLD and magnetron sputtering as oxygen electrocatalysts. In accordance with the topic, all cases employing PVD utilize perovskites as the target materials.

4.1.1.1. Enhancing bifunctional oxygen electrocatalysis. BSCF and manganite perovskites are among the most active catalysts for the OER and ORR, respectively.[10,29] The Shao-Horn group utilized PLD to fabricate a two-layer perovskite composed of BSCF and $La_{0.8}Sr_{0.2}MnO_{3-\delta}$ (LSMO) on a (001)-oriented Nb-doped $SrTiO_3$ (NSTO) substrate (Fig. 2b).[30] The fabrication of (001) oriented BSCF|LSMO|NSTO films involved two-steps. First, a 16 nm layer of LSMO was deposited on the NSTO substrate. BSCF layers with varying thicknesses (1, 2, 5, 10, and 20 nm) were subsequently deposited on the LSMO substrate, achieving BSCF surface coverages of 20%, 28%, 48%, 91%, and 94%, respectively. Electrochemical analysis revealed that these two-layer perovskite films with tunable BSCF coverage (20–91%) exhibit bifunctional oxygen electrocatalysis, where BSCF domains drive the OER kinetics while LSMO regions govern the ORR activity. As a result, the combined BSCF|LSMO|NSTO catalyst shows a comparable OER activity to BSCF powder and superior ORR activity to LSMO powder. Moreover, the BSCF decoration was confirmed to enhance the surface stability of the ORR. Furthermore, it is necessary to mention that LSMO can bring down the Schottky barrier between BSCF and NSTO, facilitating the charge transfer at the solid–solid interface. The introduction of a buffer layer is able to tailor band bending and covalency of surface near oxygen bonds.[31,32] For more details, please refer to the high-impact review paper published by the Risch research group on epitaxial perovskites for the OER.[23]

4.1.1.2. Tuning proton-coupled electron transfer (PCET) in the OER. The OER generally involves a PCET step. Modulating the PCET process can speed up the rate of the OER.[33] In a study conducted by Liu and co-workers, the PCET process was modified by tuning crystal orientation of $PrBa_{0.5}Sr_{0.5}Co_{1.5}Fe_{0.5}O_{5+\delta}$ (PBSCF) through the PLD method (Fig. 2c).[34] PBSCF thin films with well-defined orientation of (100), (110), and (111) planes are prepared on an $LaAlO_3$ single crystal substrate. Electrochemical measurements and DFT calculations consistently verified that the OER activity of PBSCF thin films follows the order of (100) > (110) > (111) planes. The outstanding activity of the (100) plane is attributed to the facilitated deprotonation process, leading to an effective PCET during the OER. The most direct evidence stems from near-ambient pressure X-ray photoelectron spectroscopy (APXPS), which definitively reveals that water deprotonation proceeds with the highest efficiency on the (100) surface. This study highlights the modification of the OER process on perovskite-based catalysts prepared by the PLD method.

4.1.1.3. Uncovering surface reconstruction. Iridium (Ir) oxide is the only known material that can operate stably in the acidic electrolyte for the OER.[35] Due to the high-cost and scarcity of

noble-metal Ir, a large amount of studies have focused on improving activity while lowering the content of Ir. In 2016, Jaramillo and coworkers prepared a $SrIrO_3$ perovskite thin film by PLD and successfully uncovered its reconstruction behavior in the acidic electrolyte (Fig. 2d).[36] The electrochemical test shows a continuously increased OER activity, which is much higher than its theoretical performance predicted from DFT calculations. Then atomic force microscopy (AFM) records the evolution of the $SrIrO_3$ surface from flat to rough. Moreover, the relative quantity of surface Sr determined by X-ray photoelectron spectroscopy (XPS) is much less than that in the subsurface layer. Based on the above observations, it is concluded that during the OER, the $SrIrO_3$ perovskite would *in situ* transform into the $IrO_x/SrIrO_3$ catalyst owing to the leaching of Sr. Specifically, it is difficult to capture such direct evidence of surface reconstruction in bulk perovskites.

Weber and coworkers systematically mapped the degradation pathways in a representative Co-based perovskite, *i.e.*, $La_{0.6}Sr_{0.4}CoO_{3-\delta}$, during alkaline OER operation, uncovering the complex surface-mediated activation–deactivation process.[37] A multiscale microscopy and spectroscopy approach reveals that the OER activity arises from the *in situ* formed CoO(OH) active layers, whereas $La(OH)_3$ passivation drives performance decay. Specifically, Sr leaching facilitates the creation of metastable mixed-phase interfaces, while Co depletion from the self-assembled CoO(OH) active layer coupled with $La(OH)_3$ accumulation ultimately leads to a gradual decrease in OER activity. This landmark study establishes the critical role of lanthanide-alkaline earth cation synergy in controlling reconstruction equilibria that dictate both activity and stability in alkaline OER catalysis.

4.1.1.4. Investigating links between activity and stability. Due to the relatively lower price and higher activity of Ru, researchers have attempted to replace Ir by Ru when designing OER catalysts.[38] Nevertheless, Ru based oxides suffer from severe degradation under OER conditions, so balancing activity and stability of Ru-based catalysts becomes the target pursued for the practical applications.[39] In 2013, with the help of magnetron sputtering, the Markovic group first prepared single-crystal $SrRuO_3$ nanofilms with three typical orientations[40] and found the OER activity following the order of (001) < (110) < (111) planes, which is inverse to their stability trend (Fig. 2e). Following this study, modification methods are employed to further improve the activity or stability of the most stable $SrRuO_3$(001) nanofilms. For instance, the phase-transformed $SrRuO_3$ (001) nanofilm induced by Ru/O vacancies results in a 30% decrease in the overpotential for the OER.[41] Furthermore, an ultrathin coating of $SrTiO_3$ on the $SrRuO_3$ nanofilms prepared through PLD demonstrated much better OER stability but a slight decrease in activity.[42]

Epitaxial stabilization of $SrRuO_3$ beneath a two-unit-cell $SrTiO_3$ overlayer achieves atomic-scale passivation, effectively suppressing corrosion of the metastable $SrRuO_3$ phase during the OER while maintaining interfacial charge transfer capabilities. PLD preparation provides convenience for investigating links between the activity and stability of perovskite catalysts. For further insights into balancing activity and stability, we recommend referring to the papers published by research groups of Bauemer and Stroerzinger.[43,44]

4.1.1.5. Controlling surface terminated cations. The surface of bulk perovskites is often enriched with A-site cations owing to their lower surface energy compared to B-site cations.[45,46] The surface enrichment of A-site cations would hinder the involvement of active B–O sites during the OER, thus suppressing the activity of perovskite catalysts. For example, although $LaNiO_3$ (LNO) is a highly efficient OER catalyst from theoretical prediction, its actual performance is far from satisfactory due to the easy enrichment of inert La at the surface.[47–52] Notably, the PVD technique can realize the regulation of surface terminated cations, adjusting catalytic behaviors. As shown in Fig. 2f, Baeumer *et al.* used the PVD technique to obtain La-terminated $LaNiO_3$ (La-LNO) and Ni-terminated $LaNiO_3$ (Ni-LNO) nanofilms (001).[53] The Ni-LNO sample shows a much better OER performance due to the easy formation of the disordered NiO_2 layer on the catalyst surface during the OER, which is inaccessible in the La-LNO counterpart. This highlights the distinct merit of the PVD method in finely controlling surface terminated cations to reduce activity loss resulting from inert-cation enrichment on the perovskite surface, which is difficult to realize in bulk perovskite materials. Subsequent work conducted by Baeumer and colleagues systematically investigated the crystallographic anisotropy of OER activity in LNO, revealing a distinct crystal-facet-dependent trend: LNO (111) > LNO (110) > LNO (001).[54] This hierarchy was attributed to the preferential formation of reconstructed oxyhydroxide-like NiOO(H) active species on the LNO (111) surface, resulting in optimized binding energy of reaction intermediates for enhanced water oxidation kinetics.

4.1.1.6. Amorphous nanofilms. Amorphous materials with an unsaturated coordination environment usually lead to enhanced OER activity.[55,56] In 2017, we utilized magnetron sputtering to prepare a series of amorphous BSCF nanofilms with varied thickness (1, 5, 10, 15, and 20 nm) at room temperature (Fig. 2g).[57] The mass activity of BSCF increased by 2 orders of magnitude owing to the largely increased atom utilization. Moreover, the intrinsic OER activity of amorphous BSCF nanofilms shows a volcano trend as a function of the film thickness, which is well-correlated with the electronic configuration of Co/Fe active sites. Following this work, we further prepared a series of perovskite-derived amorphous nanofilms *via* room temperature magnetron sputtering,[58] from which a universal rule is obtained, namely, the amorphization of perovskites accelerates the *in situ* surface reconstruction during water splitting regardless of the initial crystal structures and compositions of perovskites. Generally, amorphous nanofilms prepared by magnetron sputtering have significant advantages such as improving mass activity, fine-tuning electronic configuration and accelerating reconstruction during the OER.

4.1.2. Plasma etching - creating surface defects. Plasma etching utilizes plasma, a highly ionized gas, to remove components from the surface of perovskites (Fig. 2h). The reactive ions and radicals within the plasma interact with the perovskites, breaking chemical bonds and forming volatile byproducts that

are subsequently removed. This process inherently creates defects on the catalyst surface.[59] Maintaining the pristine structure becomes difficult with the accumulation of etching-induced defects, which eventually leads to surface amorphization.[60] Both defects and amorphization structure have significant effects on the performance of oxygen electrocatalysis.[61,62] Besides, plasma etching treatment would increase surface area or improve hydrophilicity of perovskite catalysts, facilitating the catalytic rate. The following pioneering studies demonstrate the advantages of plasma etching when disassembling and reassembling perovskites for the OER.

4.1.2.1. Creating surface cation vacancies. Perovskite hydroxide refers to a class of materials that have a perovskite-like crystal structure and contain hydroxide (OH^-) ions instead of oxygen ions (O^{2-}) in traditional perovskites. Sometimes perovskite hydroxides can be formed without A-site cations. In 2018, Wang and coworkers adopted Ar plasma to disassemble and reassemble $SnCo_{0.9}Fe_{0.1}(OH)_6$ perovskite hydroxides.[63] X-ray absorption spectral (XAS) analysis confirms that Sn vacancies are preferentially formed compared to Co and Fe, which is attributed to the lower lattice energy and weaker chemical bond in $Sn(OH)_4$. Significantly, the introduced Sn vacancies help expose more active CoFe sites and improve electron conductivity, consequently enhancing the OER performance. In addition, the specific surface area and the hydrophilicity of $SnCo_{0.9}Fe_{0.1}(OH)_6$ perovskite hydroxides are greatly improved, providing extra benefits to the OER. Later, a solution plasma was utilized to disassemble and reassemble the $SnCo(OH)_6$ perovskite hydroxides.[64] It is revealed that the OER activity of $SnCo(OH)_6$ perovskite hydroxide after solution plasma is related to the surface composition, which is determined by the pH of the solution used.

4.1.2.2. Creating oxygen vacancies. Oxygen vacancy is a key parameter to regulate the electrocatalytic performance of perovskite materials.[61] In 2018, Gui *et al.* utilized Ar plasma and created abundant oxygen vacancies on the surface of $La_{0.7}Sr_{0.3}CoO_{3-\delta}$.[65] The introduction of oxygen vacancies in $La_{0.7}Sr_{0.3}CoO_{3-\delta}$ was shown to significantly enhance its OER performance, with marked improvements in catalytic activity, reaction kinetics, and long-term stability, likely mediated by vacancy-induced electronic structure modulation. In 2019, He *et al.* adopted a different H_2/Ar plasma to treat $Bi_{0.1}(Ba_{0.5}Sr_{0.5})_{0.9}Co_{0.8}Fe_{0.2}O_{3-\delta}$ and obtained a unique structure with a crystalline core and an amorphous shell.[66] The formation of an amorphous shell is likely attributable to the reductive H_2 gas, resulting in the generation of much more oxygen vacancies and thus the degradation of the surface structure. This oxygen-vacancy-rich core–shell structure demonstrated a 1.6-fold improvement in intrinsic OER activity, which is ascribed to the enhanced exposure of electrochemically active oxygen sites. Furthermore, by adjusting operation parameters, Liu's group[67] successfully created oxygen vacancies with various concentrations on $PrBa_{0.5}Sr_{0.5}Co_{1.5}Fe_{0.5}O_{5+\delta}$ (PBSCF) perovskite thin films using H_2/Ar plasma. This study reveals that oxygen vacancies can enhance OH^- adsorption and reduce the theoretical energy barrier for O* formation on the surface, thereby accelerating OER kinetics. However, excessive oxygen vacancies also create a larger bandgap and depress the O 2p band center in PBSCF, which could potentially impede OER kinetics. By carefully balancing these competing effects, oxygen-deficient PBSCF demonstrates improved OER activity. Another highlight of this work is the combination of PLD and plasma etching for disassembling and reassembling perovskites, which offers the reference for future studies.

4.1.3. Ball milling - reducing particle size and modulating surface chemistry. Ball milling is a mechanical process used to grind materials into fine powder (Fig. 2i). Therefore, the perovskite size can be facilely tuned into sub-micrometers or nanometers through such methods, which greatly promotes the exposure of active sites.[10,68,69] After ball-milling, it is common to see a large increase in mass activity, but a slight decrease in intrinsic activity. In 2013, the Shao-Horn group revealed the surface structural change of the well-known BSCF perovskite after ball milling.[70] XAS measured in the fluorescence yield (FY) and electron yield (EY) modes unveils the local structure of the bulk and near-surface regions, respectively. After ball-milling, the Fourier-transform (FT) extended X-ray absorption fine structure (EXAFS) of BSCF showed obvious increases in the intensity of the peak assigned to the edge-sharing metal–metal bond. The edge-sharing motif is not a characteristic of the perovskite structure, suggesting a surface structural transformation generated during the ball milling process. The OER activity is sensitive to the surface structural transformation, which will be discussed in the next two sections. In 2022, Xi and coworkers revealed that ball-milling can be used to regulate the oxygen defect contents in $La_xSr_{1-x}CoO_{3-\delta}$ (LSC) perovskites.[71] The oxygen defect content of LSC increased linearly with ball milling time, and the main OER mechanism shifted between AEM–LOM–AEM, accompanied by a trend of volcano-type activity. In the ball milling method, reducing the particle size and modulating surface chemistry are realized simultaneously, which determine the geometrical activity and intrinsic activity of perovskite catalysts, respectively.

4.1.4. Summary of physical methods for disassembling and reassembling perovskites. Physical methods for disassembling and reassembling perovskites rely on specialized instruments. Their advantages lie in the ability to finely disassemble and reassemble perovskites into target states, regardless of the initial components. The PVD method can produce nanofilms with controllable thickness, atomically flat surface, exposed specific crystal plane, controllable surface terminated atom, disrupted lattice periodicity, and rich anion/cation defects. While plasma etching and ball milling are fundamentally categorized as physical techniques, these methods induce non-negligible chemical modification effects on perovskites, thereby modulating their oxygen electrocatalytic performance through defect engineering and surface chemistry modulation. PLD reliably generates perovskites as the terminal phase, whereas the structural outcomes of other methodologies exhibit process-dependent variations. Specifically, whether a magnetron sputtered product is a perovskite is determined by the operating temperature, while the product of ball milling and plasma etching is determined by the processing time/power.

Although these methods require a certain technical threshold, they offer good scalability. In the context of oxygen electrocatalysis, physical methods for disassembling and reassembling perovskites are particularly suited for fundamental research.

4.2. Chemical methods and corresponding effects

4.2.1. Exsolution - exposing and reassembling active sites. Exsolution refers to the process where compositional elements are released from the perovskite lattice to form nanoparticles (NPs) anchored on the surface, which generally occurs under reduction conditions (Fig. 3a). The formation of surface NPs would leave defects or induce reconstruction in the remaining perovskite matrix. Through tuning operation parameters, we can finely tailor the properties of exsolved NPs, such as size, composition, and population.[72] Compared with exogenous NPs, the exsolved NPs embedded into the surface of perovskite matrix are endowed with more robust heterointerfaces, more uniform particle size/distribution and more controllable compositions.[73] The discussion on exsolution is classified by specific sites in perovskites.

4.2.1.1. A-site: strong metal support interaction (SMSI). A-site cations are mostly alkali or rare earth metals with poor oxygen electrocatalytic performance. In a few cases, electrochemically active metals can be incorporated into the A site of perovskites. Silver ions (Ag^+) with a large radius often exist in the A-site of perovskites. After being treated with H_2/N_2, the single-phase $Pr_{0.475}Ba_{0.475}Ag_{0.05}MnO_{3-\delta}$ ($PBAMO_3$) perovskite was transformed into an A-site deficient layered perovskite structure decorated with Ag NPs (denoted as Ag-$PBMO_5$).[73] As expected, the interaction between surface Ag NPs and the perovskite matrix is intensified (SMSI), leading to facile electron transfer and ion migration during the ORR. As a result, the Ag-$PBMO_5$ catalyst outperforms its counterparts, *i.e.*, $PBMO_5$ catalyst, $Pr_{0.5}Ba_{0.5}MnO_{3-\delta}$ catalyst, and physically mixed Ag + $PBMO_5$ composite. Coincidentally, Irvine, a pioneer in the field of perovskite exsolution, studied the exsolution of Ni NPs from the A site of the $(Ca_{0.92}Ni_{0.04})TiO_{2.96}$ perovskite.[74] Compared to its counterpart exsolving Ni NPs from the B site of the perovskite, the Ni NPs in the A-site have a smaller size and larger population and specific surface area, as well as intensified SMSI with the perovskite matrix, leading to a better OER activity.

4.2.1.2. B-site: reorganizes surface active sites. As mentioned above, the surface of perovskites is often enriched with A-site cations, blocking the electrochemically active B-site cations. Exsolution of B-site cations could facilitate the exposure of active sites that are originally located in the subsurface layer, forming new nanostructures. For instance, an A-deficient double perovskite, $(PrBa_{0.8}Ca_{0.2})_{0.95}(Co_{1.5}Fe_{0.5})_{0.95}Co_{0.05}O_{5+\delta}$, was designed for the facile exsolution of Co/CoO_x NPs.[75] Benefiting from the tailored nanostructures at the surface, the obtained electrocatalyst shows great promise when catalyzing the ORR/OER under alkaline conditions. Furthermore, a lanthana-anchored CoFe alloy catalyst was obtained from $LaCo_{0.8}Fe_{0.2}O_{3-\delta}$ (LCF) by applying a harsher treatment (700 °C for 3 h in 5% H_2/Ar).[76] Operando XAS analysis demonstrates the transformation of CoFe species into CoFe hydroxides during the OER process. The lanthana support helps promote such transformation, contributing to an enhanced OER activity. Nevertheless, the exsolution process under a reduction atmosphere poses a safety risk. In light of this, Shao *et al.* reported an organic ligand-facilitated *in situ* exsolution method under an inert N_2 atmosphere and successfully grew CoFe nanoalloys over the BSCF perovskite, and the newly formed catalyst showed much improved OER and ORR performances.[77]

4.2.2. Exfoliation - making perovskite-derived nanosheets. Exfoliation refers to separating or peeling off thin layers/sheets

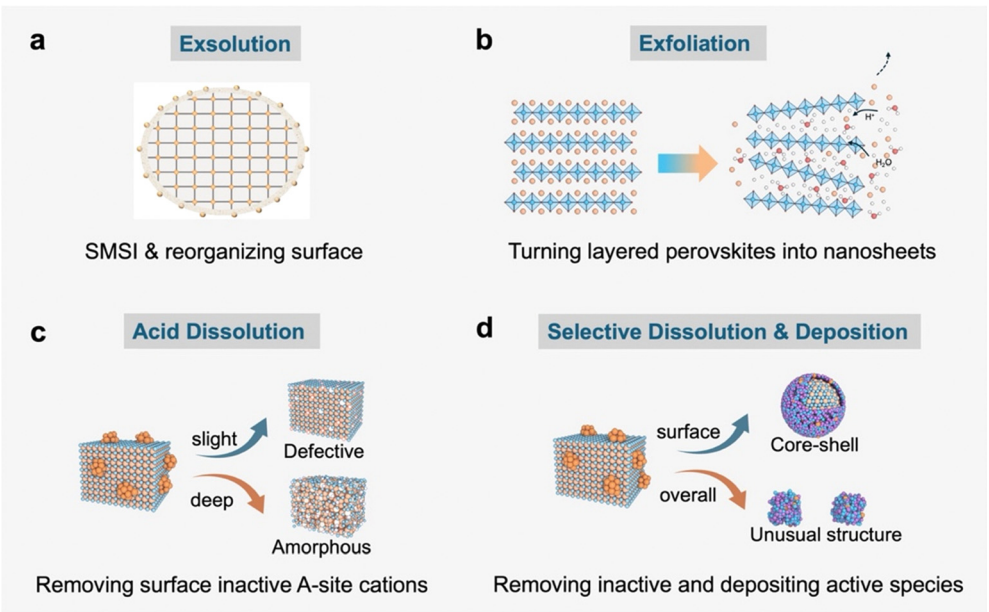

Fig. 3 Schematic illustration of chemical strategies for disassembling and reassembling perovskites. (a) The exsolution approach. (b) The exfoliation approach. (c) The acid dissolution approach. (d) The selective dissolution and deposition approaches. SMSI: strong metal–support interaction.

from bulk materials (Fig. 3b). This process cannot be applied to traditional perovskites with the general formula ABO_3 due to their three-dimensional structures. However, it is possible to exfoliate layered structured perovskites or perovskite-like materials such as Aurivillius compounds and Ruddlesden–Popper and Dion–Jacobson perovskites. As a result, two-dimensional thin slabs with a larger specific surface area, more accessible active sites, and other specific characteristics can be obtained.

4.2.2.1. Aurivillius compounds. Aurivillius compounds are a class of layered perovskite-like materials with the general formula $(Bi_2O_2)^{2+}(A_{m-1}B_mO_{3m+1})^{2-}$. These compounds feature a unique structure consisting of alternating layers of $(Bi_2O_2)^{2+}$ and perovskite-like $(A_{m-1}B_mO_{3m+1})^{2-}$ slabs. The layered structure makes them suitable for exfoliation, allowing the production of two-dimensional materials with promising oxygen electrocatalysis performance. Specifically, $CoBi_2O_2F_4$ is among the Aurivillius family.[78] The two main building units are $[CoF_6]$ octahedra and $[BiO_4F_4]$ distorted cubes. The corner-shared $[CoF_6]$ octahedra form a $[CoF_4]_\infty$ layer and the $[BiO_4F_4]$ cubes form a $[BiO_2F_2]_\infty$ layer. Using isopropanol as the solvent,[79] the exfoliation took place at the relatively weak interlayer Bi–F bonds. The exfoliation is confirmed by the corresponding SEM images in which the thickness of exfoliated $CoBi_2O_2F_4$ is only 20 to 30 nm. In addition, the exfoliation process also leads to enlarged *d*-spacing along *z*-axis dangling bonds on the edge. These features greatly improve the accessibility of Co active sites involved in the OER, leading to a decrease of 26 mV in overpotential to achieve 10 mA cm^{-2}.

4.2.2.2. Ruddlesden–Popper perovskites. Ruddlesden–Popper (RP) perovskites are a family of layered perovskite materials with the general formula $A_{n+1}B_nO_{3n+1}$ ($AO{\cdot}n(ABO_3)$), where A is typically a larger cation such as rare earth or alkaline earth metal and B is a smaller transition metal cation.[80] The integer *n* represents the number of perovskite layers between the rock-salt layers. The structure of RP perovskite consists of *n* layers of corner-sharing octahedra (ABO_3 layers) separated by rock-salt layers (AO). Such layered structure makes them suitable candidates for exfoliation, allowing the production of two-dimensional materials with promising oxygen electrocatalysis performance. Among them, Sr_2IrO_4 is a typical RP perovskite. As described in the study of the Grimaud group, the immersion of Sr_2IrO_4 in acidic solution could produce protonated iridate H_xIrO_y *via* cation exchange.[81] Then the protonated iridate was stirred in a tetrabutylammonium hydroxide (TBAOH) solution to insert TBA^+ inside the structure, followed by sonication to finally complete the exfoliation. The largely increased specific surface area of the obtained H_xIrO_y contributes obviously boosted geometrical and mass activity, while the reversible exchange of protons ensures improved catalytic stability. Another study from the Zou group realized the exfoliation of Sr_2IrO_4 without damaging the perovskite structure.[82] The 2D morphology of protonated perovskite nanosheets enables the straightforward assembly of a low-iridium-loading catalyst film, delivering a mass activity 10-fold higher than commercial IrO_2, while maintaining comparable iridium dissolution rates under OER conditions. A thermochemical dehydration method may provide a more facile route for manipulating protons in perovskites without degrading the crystal quality of perovskites.[83]

4.2.2.3. Dion–Jacobson perovskites. Dion–Jacobson (DJ) perovskites are a class of layered perovskite materials with the general formula $A'A_{n-1}B_nO_{3n+1}$, where A′ refers to a large organic or inorganic cation, A includes smaller cations such as alkali or alkaline earth metal, and B is a transition metal cation.[84] The integer *n* represents the number of perovskite layers between the A′ cation layers. In DJ perovskites, the structure consists of *n* layers of corner-sharing BO_6 octahedra (perovskite layers) separated by a single layer of A′ cations. The typical ion-exchange and subsequent exfoliation treatments used on the above RP perovskites are also applicable to bulk DJ perovskites for making $A_{n-1}B_nO_{3n+1}$ nano-slabs. For instance, bulk DJ perovskite $KCa_2Nb_{3-x}Ta_xO_{10}$ (x = 0, 0.5, 1, 1.5) can be exfoliated by sequentially subjecting to HNO_3 and TBAOH solutions.[85] The exfoliated catalyst was demonstrated to enhance H_2O_2 generation by increasing exposure of active sites, diminishing interfacial resistance and promoting charge transport.

4.2.3. Acid treatment - removing inactive cations only. Acid dissolution of perovskites involves treating perovskite materials with acid solutions to selectively dissolve certain components or impurities (Fig. 3c). This process could modify compositions and create structural changes in perovskites. Since A-site cations are more alkaline than B-site ones, acid dissolution generally prefers dissolving A-site cations, exposing B–O motifs. Slight dissolution of A-site cations might enable the creation of A-site defects only, while a severe dissolution would probably lead to reconstruction of B–O motifs. Moreover, acid leaching is also effective in improving oxygen electrocatalytic performance in protonic ceramic cells by rejuvenating the surface of solid perovskite electrolytes.[86]

4.2.3.1. Creating A-site defects. The first case is concerning slight dissolution of A-site cations, which is achieved on the $La_{0.6}Sr_{0.4}Co_{0.8}Fe_{0.2}O_3$ (LSCF) perovskite by finely controlling the acid treating time.[87] A 6-hour treatment in 0.2 M HNO_3 solution leads to the predominant dissolution of Sr^{2+} and slight dissolution of La/Co cations. Originated from the optimized surface with rich A-site defects, enlarged surface area and a large amount of active oxygen species, the mass activity and specific activity of the treated LSCF catalysts when catalyzing the OER were 6-fold and 2.6-fold higher than those of the pristine LSCF, respectively.

4.2.3.2. Reconstruction of B–O motifs. In the report from the Francisco group, when exposed to HNO_3 solution, the surface A-site cations of the LSMO perovskite were dissolved while the remaining Mn–O motifs transformed into MnO_x simultaneously, thus generating the MnO_x/LSMO composite catalyst enriched with Mn at the surface.[88] The resulting catalyst shows improved ORR performance compared to the pristine LSMO owing to the relatively higher specific surface area and much more active sites (Mn and O). Another example is Ir-based perovskites.[89] Through treatment in strong acid solution, the surface Ba cations of the 9R-$BaIrO_3$ perovskite are dissolved

with uniform IrO_x particles (1 nm) generated on the surface. The resulting IrO_x/9R-$BaIrO_3$ catalyst exhibits the highest iridium mass activity (168 A g^{-1}) among the reported iridium-based Ir perovskites for the acidic OER, which is ascribed to the abundant higher-valence Ir at the catalyst surface and the enhanced metallic conductivity.

4.2.4. Acid treatment - dissolving and depositing simultaneously. This method involves the deposition of new active species simultaneously with the dissolution of perovskite components during acidic treatment (Fig. 3d). Generally, the disparity in the redox potential or solubility of A/B elements should be considered when choosing acid solution, and significant changes in either morphology or electronic structure would take place in the perovskite materials.

4.2.4.1. Regulating the catalyst interface. Antiperovskites refer to a class of materials with the perovskite structure but reversed arrangement of cations and anions.[90] Owing to the flexibility in element composition and high electronic conductivity, antiperovskites have shown great potential in oxygen electrocatalysis. However, similar to the traditional perovskite, they also suffer from bulk characteristics resulting from sintering. In 2018, our group treated the Cu-excess $CuNNi_3$ antiperovskite ($CuNNi_3$ + Cu) with acidic $FeCl_3$ solution (pH = 2.3),[91] during which the excessive Cu particles can be oxidized to soluble Cu^{2+} ions, thus creating rich pores. Besides, metallic Cu and Ni in $CuNNi_3$ can be etched to form soluble Cu^{2+} and Ni^{2+} ions. Owing to the continuous consumption of H^+, the hydrolysis of these metal ions was promoted, leading to the deposition of amorphous FeNiCu hydroxide on the antiperovskite. The obtained core–shell composite material with a well-tailored interface shows a dramatically decreased overpotential of 300 mV to achieve 10 mA cm^{-2}. Following this research, Cui *et al.* adopted a similar approach to optimize $ZnNNi_3$ antiperovskites,[92] after which an obvious reduction in overpotential was realized on the fabricated electrode in operation of the OER.

4.2.4.2. Turning bulk perovskites into amorphous NPs. Using LN as a model material, we showed how $FeCl_3$ solution turns bulk LN perovskites into amorphous Ni–Fe based hydroxides with unique local structures.[93] The key processes are listed as follows: (i) the acidic $FeCl_3$ solution selectively dissolves alkaline La^{3+} with the depletion of H^+ (pH value gets larger); (ii) simultaneously, the corner-shared Ni^{3+}–O octahedra change into edge-shared Ni^{3+}–O octahedra; and (iii) the larger pH will promote the hydrolysis of Fe^{3+} to form FeOOH surrounded at the interstitial sites of Ni–O octahedra. As a result, the pristine bulk LN perovskite is turned into amorphous Ni–Fe-based NPs with distinguished local structures and boosted OER activity/stability.

4.2.4.3. Tailoring surface cation configuration. During the dissolution and deposition processes, surface cation configuration of catalysts can be well tailored, which plays critical roles in determining the final catalytic performance. La_2NiO_4 (L_2N) is a typical RP perovskite with an La-enriched surface.[94] We utilized $FeCl_3$ solution with various concentrations to study its influence on the RP perovskite structure.[95] When the concentration is low, a considerable amount of inert La remains, blocking active Ni sites and preventing the formation of Ni–Fe pairs. Meanwhile, excessive concentration of $FeCl_3$ solution would not only dissolve all La cations at the surface but also induce significant accumulation of FeOOH, which buries the more active Ni–Fe pairs. As expected, $FeCl_3$ treatment on La_2NiO_4 with the optimal solution concentration leads to the desirable surface cation configuration. Both the OER activity and stability of treated samples show a volcano-shaped dependence on the atomic ratio of (Ni + Fe)/La at the surface. The optimized catalyst with the (Ni + Fe)/La value close to unity demonstrates the best OER activity/stability among all RP based perovskites thus far.

4.2.5. Summary of chemical approaches for disassembling and reassembling perovskites. Exfoliation always destroys the perovskite structure, resulting in a layered nanosheet material. The products of exsolution and acid treatment can be divided into defective perovskites and perovskite derivatives (non-perovskites) according to the degree of treatment. Many other chemical approaches have also been employed when disassembling and reassembling perovskites for optimizing oxygen electrocatalysis. For instance, the Li-reduction strategy induced surface amorphization of perovskites, enhancing OER and ORR activities simultaneously.[96] Compared with physical approaches, chemical methods seldom rely on specialized instruments, require a gaseous or liquid environment only, are easily scalable, and can be used to tailor other materials beyond perovskites.[97–101]

4.3. Electrochemical approaches and corresponding effects

Electrochemical leaching is a scientific term describing the process during which a soluble component is separated or extracted from its carrier/substance and transferred into electrolyte driven by electro-potentials. The Pourbaix diagrams (potential–pH diagrams) provide precise information for element leaching in aqueous systems based on equilibrium thermodynamics.[28] When exposed to applied potentials, metastable species characterized by fragile bonds in the initial structure and solubility in electrolyte would easily detach from the perovskite lattice and dissolve into the electrolyte.[28] This leads to the disruption of the original perovskite structure, the creation of defects and the greater exposure of the solid–liquid interface, namely, surface reconstruction (Fig. 4). Generally, electrochemical leaching is more prevalent in complex oxides such as perovskites owing to their rich elemental composition and diverse chemical properties. In the following sections, disassembling and reassembling perovskites through electrochemical leaching and reconstruction are summarized based on distinct electrochemical reactions.

4.3.1. OER in alkaline electrolyte. BSCF is an emerging perovskite material in electrochemistry.[102] It was initially used for preparing well-performing oxygen ionic transport membranes or cathode materials in solid oxide fuel cells at high temperatures.[103] In recent years, it has been well recognized as an efficient OER catalyst at temperatures below 100 °C.[10] Specifically, it was found that the OER activity of BSCF increased with electrochemical cycling, during which the leaching of Ba^{2+}/Sr^{2+} and amorphization

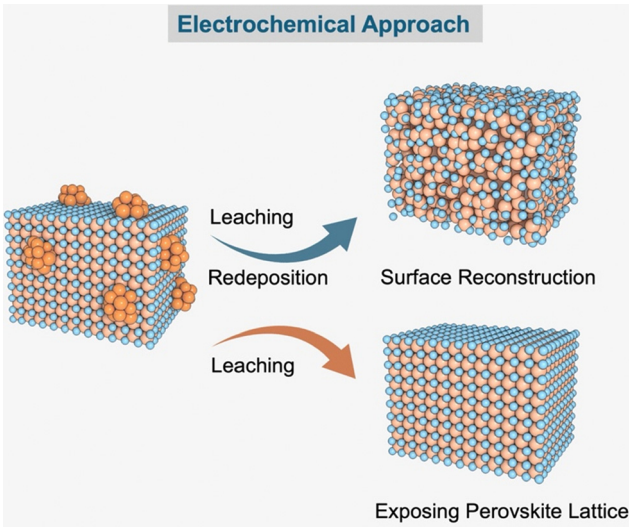

Fig. 4 Schematic illustration of the electrochemical strategy for disassembling and reassembling perovskites.

of the catalyst surface took place.[70] In sharp contrast, perovskite catalysts with poor OER activity such as $LaCoO_3$ did not undergo such transformations. Using time-resolved XAS, the Schmidt group captured the dynamic local structure of BSCF during the OER process.[13] The surface reconstruction process can be described as follows: the highly soluble Ba^{2+}/Sr^{2+} leached out from the perovskite structure and stayed in the electrolyte during the OER. The Co/Fe species also leached out but would redeposit back as Co/Fe(O)OH, driven by the external potentials. Finally, the dynamic surface reconstruction with the formation of active Co/Fe(O)OH species is the key for outstanding OER performance. Another study conducted by Markovic *et al.* confirmed that the highly active hydr(oxy)oxide layer on the surface of perovskite originates from electrochemical reconstruction driven by A-site leaching and creation of oxygen vacancies.[104] Trace-level Fe species in the electrolyte accelerate the above process to form dynamically stable hydr(oxy)oxide sites, boosting OER activity and stability.

4.3.2. OER in acidic electrolytes. Iridium oxide is the only known material that can operate stably in acidic electrolyte for the OER. Koper *et al.* first reported the application of iridium-based perovskites as OER catalysts in acidic media.[105] Since the report about Sr leaching in the $SrIrO_3$ perovskite during the acidic OER process,[35] surface reconstruction of iridates has been widely investigated. Regarding the big problem of stability, Cherevko and coworkers explored the dissolution process of various iridium-based oxides and introduced the concept of stability number,[14] which could serve as a metric for stability benchmarking of electrocatalysts, allowing illustrative and quick comparison of stability property and direct evaluation of lifetime and providing insights into degradation mechanisms. Grimaud *et al.* proposed that besides the non-precious metal ions, Ir also participated in the dynamic dissolution–redeposition process during the OER.[106] The dissolution/redeposition equilibrium of Ir of iridates controls the final OER activity. Very recently, the Seitz group identified the formation of paracrystalline motifs on iridate surfaces during the OER process using advanced X-ray/electron scattering techniques.[15] This study has addressed the long-standing issues regarding the structure and chemical properties of highly active IrO_x motifs that are derived from crystalline iridates.

Besides, many studies focus on using iridium-based perovskites as OER catalysts to reduce the Ir content and utilize component leaching to form the more active Ir motifs. The Xu group reported the surface reconstruction of B-site doped $SrIrO_3$ perovskites by non-noble metals.[107,108] The B-site substitution further reduces the content of Ir, thus reducing the price of the catalyst. What's more, the non-noble B-site cations leach out together with the A-site Sr cations, further promoting the degree of surface reconstruction. Specifically, the $SrCo_{0.9}Ir_{0.1}O_3$ perovskite shows obvious surface reconstruction on its surface region.[107] The reconstructed corner-shared and under-coordinated IrO_x octahedra are responsible for the exceptionally high OER activity. A further study shows that the A-site cation leaching generates more electrochemical surface area for the reaction, and additional leaching of B-site induces the formation of a honeycomb-like IrO_xH_y phase, significantly enhancing the intrinsic activity.[108] The reconstructed IrO_xH_y motifs show an activity improvement by approximately two orders of magnitude compared to the pristine counterpart. For more related studies please refer to ref. 109–111.

4.3.3. ORR process. Owing to the intrinsic disparity between A and B site cations, the surface of perovskites often deviates from its ideal structure and consists of enriched A-site cations. This feature brings challenges to the establishment of precise structure–activity relationship of perovskite catalysts. Typically, the surface of $AgNbO_3$ presents as Ag NPs embedded in an Ag-deficient perovskite structure.[112] We applied oxidation potentials on $AgNbO_3$ under alkaline conditions and realized the dissolution of Nb species based on the Pourbaix diagram of $AgNbO_3$.[113] Without a foothold, the embedded Ag NPs at the surface fell down in solid form. High-resolution TEM images revealed the exposure of the perovskite lattice of $AgNbO_3$ after such treatment. As a result, the electrochemically treated $AgNbO_3$ material shows much improved $2e^-$ ORR activity and selectivity. Combining theoretical calculations and experimental data, it is demonstrated that the isolated Ag active sites in the perovskite lattice are responsible for the highly active and selective $2e^-$ ORR performance, while the Ag NPs account for the $4e^-$ ORR route. By disassembling perovskites *via* the electrochemical oxidation, this work realized the exposure of the perovskite lattice for efficient production of H_2O_2. For a broader context, perovskites can be expected to be employed as platforms for creating isolated active sites to realize the targeted synthesis of small molecules.

4.3.4. Summary of electrochemical approaches for disassembling and reassembling perovskites. The structural evolution of perovskite systems is electrochemically mediated through three governing parameters: elemental composition, electrolyte pH, and applied potential. These variables collectively drive two distinct transformation pathways: (1) phase reconstruction involving perovskite disassembly into reactive hydroxide species or (2) surface polishing through removal of surface non-ideal layers, thereby exposing pristine lattice structures. Disassembling and reassembling perovskites using electrochemical methods represents a

significant advance in the field of oxygen electrocatalysis. It helps reveal the dynamic reconstruction characteristics of catalysts and provides crucial insights when establishing structure–activity relationships for future design of more efficient catalysts. Theoretically, electrochemical disassembling and reassembling relies on the guidance of Pourbaix diagrams, while experimentally, it generally requires the support from various *in situ* characterization methods. This approach has the highest threshold.

5. Conclusion and perspectives

In this minireview, we give a summary regarding disassembling and reassembling perovskites including their definition, benefits, approaches, and applications in oxygen electrocatalysis. Representative examples illustrate how the disassembling and reassembling perovskites effectively tackle the major challenges faced by original perovskite catalysts. The disassembling and reassembling strategy aims to engineer electrochemical active sites through two synergistic approaches: precisely tailoring intrinsic active sites within perovskite architectures, while strategically generating extrinsic active sites in perovskite-derived matrices. Notably, even the pre-engineered active sites in parent perovskites may experience dynamic transformations during electrocatalytic operation, ultimately evolving into emergent active sites through structural restructuring. Significant breakthroughs including the revealing of dynamic surface reconstruction, proposal of stability number, and the findings about paracrystalline motifs on reconstructed iridium oxides are highlighted. Among the three methods of disassembling and reassembling perovskites, the physical method allows more precise control of structure properties, making it suitable for fundamental studies. The chemical method is straightforward and effective and holds promise for large-scale catalyst production. Significantly, the electrochemical pathway refers to critical processes applied on catalysts under operational conditions, which hold great importance and promise for future related investigations. Despite significant advances, several scientific issues still remain in this emerging field, particularly concerning the electrochemical method:

(1) Amorphous or paracrystalline phase?

For a long time, new species generated from electrochemical reconstruction are considered amorphous by default. However, very recently, the newly generated IrO_x species *in situ* formed on Ir-based perovskites are identified paracrystalline with short-to-medium-range-order structure rather than the amorphous phase.[15] This revelation enables theoretical modeling for corresponding DFT calculations, which is difficult to realize for amorphous cases. It is thus imperative to re-evaluate the reconstructed process and products for perovskite catalysts, which would help establish more accurate structure–activity relationships advancing the unveiling of reaction mechanisms and promoting practical applications for hydrogen production.

(2) Deteriorated interfaces between perovskites and ionomers

Disassembling and reassembling perovskites by the electrochemical method generally involves *in situ* leaching and redeposition processes, which are often accompanied by evolution of morphology or reduction of particle size. However, accordingly the catalytic activity often follows the trend that first increases and then decreases. The activity decay may result from the deteriorated interface between catalyst and ionomer, which would reduce ion conductivity, decrease electron transfer efficiency, and increase electrochemical resistance. The underlying mechanism needs to be investigated and corresponding strategies must be developed to prevent the interfacial degradation, so as to ensure long-term operation when enjoying the benefits of disassembling and reassembling perovskites.

(3) Directed by artificial intelligence (AI)

Predicting highly efficient catalyst materials using AI should result in a higher efficiency than that obtained using the traditional trial and error methods. However, considering the existence of electrochemical reconstruction, candidate materials predicted by AI at present should act as pre-catalysts in oxygen electrocatalysis, but not real-catalysts. As we have summarized in the electrochemical methods for disassembling and reassembling perovskites, there are remarkable property differences between pristine perovskite and electrochemically reconstructed products. From this perspective, if AI prediction is based on real-catalysts rather than pre-catalysts, it would give us a more accurate direction when developing target catalysts.

(4) Extending applications beyond oxygen electrocatalysis

Perovskite materials have been widely applied in the field of energy conversion and storage. Besides oxygen electrocatalysis, large surface area and favorable structure are also essential properties for other electrochemical processes. Considering the various strategies and obvious advantages when disassembling and reassembling perovskites, it should bring more opportunities in extending applications beyond oxygen electrocatalysis. For example, in carbon electrocatalysis (CO_2 reduction and organics conversion), dynamically restructured interfaces enable multi-carbon pathway control *via* metastable intermediate stabilization. For nitrogen cycling applications (N_2 fixation and nitrate reduction), the multi-component active sites can be responsible for nitrogen dissociation and protonation, respectively, breaking scaling relations through spatially decoupled reaction steps.

Data availability

No primary research results, software or code have been included and no new data were generated or analysed as part of this review.

Conflicts of interest

The authors declare that they have no known competing financial interests or personal relationships that could have appeared to influence the work reported in this paper.

Acknowledgements

This work was supported by the Program for Jiangsu Specially-Appointed Professors (R2023T05), the Startup Foundation for

Introducing Talent of NUIST (2024R078), the Natural Science Foundation of Jiangsu Province (BK20240707, BK20241425), and the National Natural Science Foundation of China (No. 22278203).

References

1 Y. Chen, D. J. Zheng, Z. J. Xu and Y. Shao-Horn, *Nat. Sustainability*, 2024, **7**, 371.
2 H. Yang, X. Han, A. I. Douka, L. Huang, L. Gong, C. Xia, H. S. Park and B. Y. Xia, *Adv. Funct. Mater.*, 2021, **31**, 2007602.
3 Z. Wang, Y.-R. Zheng, I. Chorkendorff and J. K. Nørskov, *ACS Energy Lett.*, 2020, **5**, 2905.
4 W. T. Hong, M. Risch, K. A. Stoerzinger, A. Grimaud, J. Suntivich and Y. Shao-Horn, *Energy Environ. Sci.*, 2015, **8**, 1404.
5 P. Gayen, S. Saha and V. Ramani, *Acc. Chem. Res.*, 2022, **55**, 2191.
6 J. Hwang, R. R. Rao, L. Giordano, Y. Katayama, Y. Yu and Y. Shao-Horn, *Science*, 2017, **358**, 751.
7 J. Moon, W. Beker, M. Siek, J. Kim, H. S. Lee, T. Hyeon and B. A. Grzybowski, *Nat. Mater.*, 2024, **23**, 108.
8 C. Shang, X. Xiao and Q. Xu, *Coord. Chem. Rev.*, 2023, **485**, 215109.
9 X. Liang, W. Yan, Y. Yu, K. Zhang, W. An, H. Chen, Y. Zou, X. Zhao and X. Zou, *Angew. Chem., Int. Ed.*, 2023, **62**, 202311606.
10 J. Suntivich, K. J. May, H. A. Gasteiger, J. B. Goodenough and Y. Shao-Horn, *Science*, 2011, **334**, 1383.
11 J. T. Mefford, X. Rong, A. M. Abakumov, W. G. Hardin, S. Dai, A. M. Kolpak, K. P. Johnston and K. J. Stevenson, *Nat. Commun.*, 2016, **7**, 11053.
12 A. Grimaud, O. Diaz-Morales, B. Han, W. T. Hong, Y. L. Lee, L. Giordano, K. A. Stoerzinger, M. T. Koper and Y. Shao-Horn, *Nat. Chem.*, 2017, **9**, 457.
13 E. Fabbri, M. Nachtegaal, T. Binninger, X. Cheng, B. J. Kim, J. Durst, F. Bozza, T. Graule, R. Schäublin, L. Wiles and M. Pertoso, *Nat. Mater.*, 2017, **16**, 925.
14 S. Geiger, O. Kasian, M. Ledendecker, E. Pizzutilo, A. M. Mingers, W. T. Fu, O. Diaz-Morales, Z. Li, T. Oellers, L. Fruchter and A. Ludwig, *Nat. Catal.*, 2018, **1**, 508.
15 B. Lu, C. Wahl, R. dos Reis, J. Edgington, X. K. Lu, R. Li, M. E. Sweers, B. Ruggiero, G. K. K. Gunasooriya, V. Dravid and L. C. Seitz, *Nat. Catal.*, 2024, **7**, 868.
16 X. Xu, W. Wang, W. Zhou and Z. Shao, *Small Methods*, 2018, **2**, 1800071.
17 B. Koo, K. Kim, J. K. Kim, H. Kwon, J. W. Han and W. Jung, *Joule*, 2018, **2**, 1476.
18 Y. Li, W. Zhang, Y. Zheng, J. Chen, B. Yu, Y. Chen and M. Liu, *Chem. Soc. Rev.*, 2017, **46**, 6345.
19 H. J. Song, H. Yoon, B. Ju and D.-W. Kim, *Adv. Energy Mater.*, 2021, **11**, 2002428.
20 C. Wu, X. Wang, Y. Tang, H. Zhong, X. Zhang, A. Zou, J. Zhu, C. Diao, S. Xi, J. Xue and J. Wu, *Angew. Chem., Int. Ed.*, 2023, **52**, 202218599.
21 C. H. Park, H. Lee, J.-S. Choi, T. G. Yun, Y. Lim, H. B. Bae and S. Y. Chung, *Adv. Mater.*, 2024, **36**, 2403392.
22 H. Sun, H. Kim, X. Xu, L. Fei, W. Jung and Z. Shao, *Renewables*, 2023, **1**, 21.
23 D. Antipin and M. Risch, *J. Phys. Energy*, 2020, **2**, 032003.
24 Z. Sun, W. Fan and T. Lin, *J. Mater. Chem. A*, 2023, **11**, 24982.
25 H. Guo, Y. Yang, G. Yang, X. Cao, N. Yan, Z. Li, E. Chen, L. Tang, M. Peng, L. Shi, S. Xie, H. Tao, C. Xu, Y. Zhu., X. Fu, Y. Pan, N. Chen, J. Lin, X. Tu, Z. Shao and Y. Sun, *ACS Catal.*, 2023, **13**, 5007.
26 Y. Ebina, T. Sasaki and M. Watanabe, *Solid State Ionics*, 2002, **151**, 177.
27 H. Li, Y. Chen, J. Z. Y. Seow, C. Liu, A. C. Fisher, J. W. Ager and Z. J. Xu, *Small Sci.*, 2022, **2**, 2100048.
28 G. Chen, Y. Zhu, S. She, Z. Lin, H. Sun and H. Huang, *InfoMat*, 2024, **6**, e12609.
29 A. Grimaud, C. E. Carlton, M. Risch, W. T. Hong, K. J. May and Y. Shao-Horn, *J. Phys. Chem. C*, 2013, **117**, 259262.
30 M. Risch, K. A. Stoerzinger, S. Maruyama, W. T. Hong, I. Takeuchi and Y. Shao-Horn, *J. Am. Chem. Soc.*, 2014, **136**, 5229.
31 J. D. Baniecki, H. Yamaguchi, C. Harnagea, D. Ricinschi, Z. Gu, J. E. Spanier, T. Yamazaki and H. Aso, *Adv. Energy Mater.*, 2019, **9**, 1803846.
32 L. Heymann, M. L. Weber, M. Wohlgemuth, M. Risch, R. Dittmann, C. Baeumer and F. Gunkel, *ACS Appl. Mater. Interfaces*, 2022, **14**, 14129–14136.
33 D. G. Nocera, *J. Am. Chem. Soc.*, 2022, **144**, 1069.
34 Y. Zhu, Z. He, Y. Choi, H. Chen, X. Li, B. Zhao, Y. Yu, H. Zhang, K. A. Stoerzinger, Z. Feng, Y. Chen and M. Liu, *Nat. Commun.*, 2020, **11**, 4299.
35 C. Wei, Z. Wang, K. Otani, D. Hochfilzer, K. Zhang, R. Nielsen, I. Chorkendorff and J. Kibsgaard, *ACS Catal.*, 2023, **13**, 14058.
36 L. C. Seitz, C. F. Dickens, K. Nishio, Y. Hikita, J. Montoya, A. Doyle, C. Kirk, A. Vojvodic, H. Y. Hwang, J. K. Norskov and T. F. Jaramillo, *Science*, 2016, **353**, 1011.
37 M. L. Weber, G. Lole, A. Kormanyos, A. Schwiers, L. Heymann, F. D. Speck, T. Meyer, R. Dittmann, S. Cherevko, C. Jooss, C. Baeumer and F. Gunkel, *J. Am. Chem. Soc.*, 2022, **144**, 17966–17979.
38 S. Li, S. Zhao, F. Hu, L. Li, J. Ren, L. Jiao, S. Ramakrishna and S. Peng, *Prog. Mater. Sci.*, 2024, **145**, 101294.
39 N. Danilovic, R. Subbaraman, K. C. Chang, S. H. Chang, Y. Kang, J. Snyder, A. P. Paulikas, D. Strmcnik, Y. T. Kim, D. Myers and V. R. Stamenkovic, *Angew. Chem., Int. Ed.*, 2014, **53**, 14016.
40 S. H. Chang, N. Danilovic, K.-C. Chang, R. Subbaraman, A. P. Paulikas, D. D. Fong, M. J. Highland, P. M. Baldo, V. R. Stamenkovic, J. W. Freeland, J. A. Eastman and N. M. Markovic, *Nat. Commun.*, 2014, **5**, 4191.
41 S. A. Lee, S. Oh, J.-Y. Hwang, M. Choi, C. Youn, J. W. Kim, S. H. Chang, S. Woo, J.-S. Bae, S. Park, Y.-M. Kim, S. Lee, T. Choi, S. W. Kim and W. S. Choi, *Energy Environ. Sci.*, 2017, **10**, 924.
42 A. R. Akbashev, L. Zhang, J. T. Mefford, J. Park, B. Butz, H. Luftman, W. C. Chueh and A. Vojvodic, *Energy Environ. Sci.*, 2018, **11**, 1762.

43 M. Wohlgemuth, M. L. Weber, L. Heymann, C. Baeumer and F. Gunkel, *Front. Chem.*, 2022, **10**, 913419.
44 M. Vitale-Sullivan and K. A. Stoerzinger, *Curr. Opin. Electrochem.*, 2023, **39**, 101252.
45 B. Koo, K. Kim, J. K. Kim, H. Kwon, J. W. Han and W. Jung, *Joule*, 2018, **2**, 1476.
46 Y. Li, W. Zhang, Y. Zheng, J. Chen, B. Yu, Y. Chen and M. Liu, *Chem. Soc. Rev.*, 2017, **46**, 6345.
47 I. C. Man, H.-Y. Su, F. Calle-Vallejo, H. A. Hansen, J. I. Martínez, N. G. Inoglu, J. Kitchin, T. F. Jaramillo, J. K. Nørskov and J. Rossmeisl, *ChemCatChem*, 2011, **3**, 1159.
48 J. S. Yoo, X. Rong, Y. Liu and A. M. Kolpak, *ACS Catal.*, 2018, **8**, 4628.
49 W. Zhou and J. Sunarso, *J. Phys. Chem. Lett.*, 2013, **4**, 2982.
50 J. Chen, J. Wu, Y. Liu, X. Hu and D. Geng, *Phys. Status Solidi A*, 2018, **215**, 1800380.
51 N. I. Kim, J. Lee, S. Jin, J. Park, J.-Y. Jeong, J. Lee, Y. Kim, C. Kim and S. M. Choi, *Small Methods*, 2024, **8**, 2400284.
52 J. R. Petrie, V. R. Cooper, J. W. Freeland, T. L. Meyer, Z. Zhang, D. A. Lutterman and H. N. Lee, *J. Am. Chem. Soc.*, 2016, **138**, 2488.
53 C. Baeumer, J. Li, Q. Lu, A. Y.-L. Liang, L. Jin, H. P. Martins, T. Duchoň, M. Glöß, S. M. Gericke, M. A. Wohlgemuth, M. Giesen, E. E. Penn, R. Dittmann, F. Gunkel, R. Waser, M. Bajdich, S. Nemšák, J. T. Mefford and W. C. Chueh, *Nat. Mater.*, 2021, **20**, 674.
54 A. Füngerlings, M. Wohlgemuth, D. Antipin, E. van der Minne, E. M. Kiens, J. Villalobos, M. Risch, F. Gunkel, R. Pentcheva and C. Baeumer, *Nat. Commun.*, 2023, **14**, 8284.
55 J. Kang, X. Yang, Q. Hu, Z. Cai, L. M. Liu and L. Guo, *Chem. Rev.*, 2023, **123**, 8859.
56 H. Sun, X. Xu, G. Chen and Z. Shao, *Carbon Energy*, 2024, **6**, e595.
57 G. Chen, W. Zhou, D. Guan, J. Sunarso, Y. Zhu, X. Hu, W. Zhang and Z. Shao, *Sci. Adv.*, 2017, **3**, 1603206.
58 G. Chen, Z. Hu, Y. Zhu, B. Gu, Y. Zhong, H.-J. Lin, C.-T. Chen, W. Zhou and Z. Shao, *Adv. Mater.*, 2018, **30**, 1804333.
59 K. Wang, J. Zhou, L. Fu, Y. Kang, Z. Zhou, Y. Cheng, K. Wu and Y. Yamauchi, *Small*, 2024, **20**, 2404239.
60 H. He, D. Huang, W. Pang, D. Sun, Q. Wang, Y. Tang, X. Ji, Z. Guo and H. Wang, *Adv. Mater.*, 2018, **30**, 1801013.
61 D. Yan, Y. Li, J. Huo, R. Chen, L. Dai and S. Wang, *Adv. Mater.*, 2017, **29**, 1606459.
62 S. Anantharaj and S. Noda, *Small*, 2020, **16**, 1905779.
63 D. Chen, M. Qiao, Y.-R. Lu, L. Hao, D. Liu, C.-L. Dong, Y. Li and S. Wang, *Angew. Chem., Int. Ed.*, 2018, **57**, 8691.
64 M. Narahara, S. Y. Lee, K. Sasaki, K. Fukushima, K. Tanaka, S. Chae, X. Hu, G. Panomsuwan and T. Ishizaki, *Sustainable Energy Fuels*, 2023, **7**, 2582.
65 Y. Lu, A. Ma, Y. Yu, R. Tan, C. Liu, P. Zhang, D. Liu and J. Gui, *ACS Sustainable Chem. Eng.*, 2018, **7**, 2906.
66 J. Sun, Z. Zhang, Y. Gong, H. Wang, R. Wang, L. Zhao and B. He, *Sci. Rep.*, 2019, **9**, 4210.
67 Y. Zhu, L. Zhang, B. Zhao, H. Chen, X. Liu, R. Zhao, X. Wang, J. Liu, Y. Chen and M. Liu, *Adv. Funct. Mater.*, 2019, **29**, 1901783.
68 G. Chen, Z. Hu, Y. Zhu, Z.-G. Chen, Y. Zhong, H.-J. Lin, C.-T. Chen, L. H. Tjeng, W. Zhou and Z. Shao, *J. Mater. Chem. A*, 2018, **6**, 9854.
69 Y. Zhu, W. Zhou, Z.-G. Chen, Y. Chen, C. Su, M. O. Tadé and Z. Shao, *Angew. Chem., Int. Ed.*, 2015, **54**, 3897.
70 M. Risch, A. Grimaud, K. J. May, K. A. Stoerzinger, T. J. Chen, A. N. Mansour and Y. Shao-Horn, *J. Phys. Chem. C*, 2013, **117**, 8628.
71 M. Lu, Y. Zheng, Y. Hu, B. Huang, D. Ji, M. Sun, J. Li, Y. Peng, R. Si, P. Xi and C.-H. Yan, *Sci. Adv.*, 2022, **8**, 3563.
72 X. Sun, H. Chen, Y. Yin, M. T. Curnan, J. W. Han, Y. Chen and Z. Ma, *Small*, 2021, **17**, 2005383.
73 Y.-Q. Zhang, H.-B. Tao, J. Liu, Y.-F. Sun, J. Chen, B. Hua, T. Thundat and J.-L. Luo, *Nano Energy*, 2017, **38**, 392.
74 S. Zuo, Y. Liao, C. Wang, A. B. Naden and J. T. Irvine, *Small*, 2024, **20**, 2308867.
75 B. Hua, M. Li, Y.-F. Sun, Y.-Q. Zhang, N. Yan, J. Chen, T. Thundat, J. Li and J.-L. Luo, *Nano Energy*, 2017, **32**, 247.
76 S. Song, J. Zhou, X. Su, Y. Wang, J. Li, L. Zhang, G. Xiao, C. Guan, R. Liu, S. Chen and H. J. Lin, *Energy Environ. Sci.*, 2018, **11**, 2945.
77 Y. Arafat, M. R. Azhar, Y. Zhong, R. O'Hayre, M. O. Tadé and Z. Shao, *J. Mater. Chem. A*, 2023, **11**, 12856.
78 E. Mitoudi-Vagourdi, S. Müllner, P. Lemmens, R. K. Kremer and M. Johnsson, *Inorg. Chem.*, 2018, **57**, 9115.
79 X. Yu, E. Mitoudi-Vagourdi and M. Johnsson, *ChemCatChem*, 2019, **11**, 6105.
80 C. Cao, C. Shang, X. Li, Y. Wang, C. Liu, X. Wang, S. Zhou and J. Zeng, *Nano Lett.*, 2020, **20**, 2837.
81 R. Zhang, P. E. Pearce, V. Pimenta, J. Cabana, H. Li, D. Alves Dalla Corte, A. M. Abakumov, G. Rousse, D. Giaume, M. Deschamps and A. Grimaud, *Chem. Mater.*, 2020, **32**, 3499.
82 H. Chen, L. Shi, K. Sun, K. Zhang, Q. Liu, J. Ge, X. Liang, B. Tian, Y. Huang, Z. Shi, Z. Wang, W. Zhang, M. Liu and X. Zou, *ACS Catal.*, 2022, **12**, 8658.
83 H. Chen, Z. Xu, L. Wei, M. Dong, Y. Hu, Y. Lu, N. Zhang, J. Wu and Q. Lu, *J. Mater. Chem. A*, 2024, **12**, 23658.
84 H. Fukuoka, T. Isami and S. Yamanaka, *J. Solid State Chem.*, 2000, **151**, 40.
85 X. Yang, Y. Gao, X. Xu, W. Xu, D. Wang, B. Luo, D. Liu, T. Liang and B. Wang, *Nano Res.*, 2024, **17**, 4934.
86 W. Bian, W. Wu, B. Wang, W. Tang, M. Zhou, C. Jin, H. Ding, W. Fan, Y. Dong, J. Li and D. Ding, *Nature*, 2022, **604**, 479.
87 W. Guo, L. Cui, H. Xu and C. Gong, *Appl. Surf. Sci.*, 2020, **529**, 147165.
88 J. Yu, D. Chen, M. Saccoccio, K. Lam and F. Ciucci, *ChemElectroChem*, 2018, **5**, 1105.
89 N. Li, L. Cai, C. Wang, Y. Lin, J. Huang, H. Sheng, H. Pan, W. Zhang, Q. Ji, H. Duan, W. Hu, W. Zhang, F. Hu, H. Tan, Z. Sun, B. Song, S. Jin and W. Yan, *J. Am. Chem. Soc.*, 2021, **143**, 18001.
90 K. T. Lai, I. Antonyshyn, Y. Prots and M. Valldor, *J. Am. Chem. Soc.*, 2017, **139**, 9645.
91 Y. Zhu, G. Chen, Y. Zhong, Y. Chen, N. Ma, W. Zhou and Z. Shao, *Nat. Commun.*, 2018, **9**, 1.

92 J. Zhang, J. Liu, L. Zhang, J. Ke, C. Zhong, Y. Tu, L. Wang, H. Song, L. Du, Z. Zhang and Z. Cui, *ACS Catal.*, 2023, **13**, 5043.
93 G. Chen, Y. Zhu, H. M. Chen, Z. Hu, S.-F. Hung, N. Ma, J. Dai, H.-J. Lin, C.-T. Chen, W. Zhou and Z. Shao, *Adv. Mater.*, 2019, **31**, 1900883.
94 J. Wu, S. S. Pramana, S. J. Skinner, J. A. Kilner and A. P. Horsfield, *J. Mater. Chem. A*, 2015, **3**, 23760.
95 Y. Li, G. Chen, H. C. Chen, Y. Zhu, L. Fei, L. Xu, T. Liu, J. Dai, H. Huang, W. Zhou and Z. Shao, *Energy Environ. Sci.*, 2023, **16**, 3331.
96 G. Ou, C. Yang, Y. Liang, N. Hussain, B. Ge, K. Huang, Y. Xu, H. Wei, R. Zhang and H. Wu, *Small Methods*, 2019, **3**, 1800279.
97 L. Gui, G. Pan, X. Ma, M. You, B. He, Z. Yang, J. Sun, W. Zhou, J. Xu and L. Zhao, *Appl. Surf. Sci.*, 2021, **543**, 148817.
98 F. Song and X. Hu, *Nat. Commun.*, 2014, **5**, 4477.
99 M. Yu, K. S. Belthle, C. Tüysüz and H. Tüysüz, *J. Mater. Chem. A*, 2019, **7**, 23130.
100 Y. Li, G. Chen, Y. Zhu, Z. Hu, T.-S. Chan, S. She, J. Dai, W. Zhou and Z. Shao, *Adv. Funct. Mater.*, 2021, **31**, 2103569.
101 G. Ou, Y. Xu, B. Wen, R. Lin, B. Ge, Y. Tang, Y. Liang, C. Yang, K. Huang, D. Zu, R. Yu, W. Chen, J. Li, H. Wu, L.-M. Liu and Y. Li, *Nat. Commun.*, 2018, **9**, 1302.
102 W. Zhou, R. Ran and Z. Shao, *J. Power Sources*, 2009, **192**, 231.
103 Z. Shao and S. M. Haile, *Nature*, 2004, **431**, 170.
104 P. P. Lopes, D. Y. Chung, X. Rui, H. Zheng, H. He, P. Farinazzo Bergamo Dias Martins, D. Strmcnik, V. R. Stamenkovic, P. Zapol, J. F. Mitchell, R. F. Klie and N. M. Markovic, *J. Am. Chem. Soc.*, 2021, **143**, 2741.
105 O. Diaz-Morales, S. Raaijman, R. Kortlever, P. J. Kooyman, T. Wezendonk, J. Gascon, W. T. Fu and M. T. M. Koper, *Nat. Commun.*, 2016, **7**, 12363.
106 R. Zhang, N. Dubouis, M. Ben Osman, W. Yin, M. T. Sougrati, D. A. D. Corte, D. Giaume and A. Grimaud, *Angew. Chem., Int. Ed.*, 2019, **58**, 4571.
107 Y. Chen, H. Li, J. Wang, Y. Du, S. Xi, Y. Sun, M. Sherburne, J. W. Ager III, A. C. Fisher and Z. J. Xu, *Nat. Commun.*, 2019, **10**, 572.
108 Y. Chen, Y. Sun, M. Wang, J. Wang, H. Li, S. Xi, C. Wei, P. Xi, G. E. Sterbinsky, J. W. Freeland, A. C. Fisher, J. W. Ager III, Z. Feng and Z. J. Xu, *Sci. Adv.*, 2021, **7**, 1788.
109 L. An, C. Wei, M. Lu, H. Liu, Y. Chen, G. G. Scherer, A. C. Fisher, P. Xi, Z. J. Xu and C.-H. Yan, *Adv. Mater.*, 2021, **33**, 2006328.
110 H. J. Song, H. Yoon, B. Ju and D.-W. Kim, *Adv. Energy Mater.*, 2021, **11**, 2002428.
111 Z. Lei, T. Wang, B. Zhao, W. Cai, Y. Liu, S. Jiao, Q. Li, R. Cao and M. Liu, *Adv. Energy Mater.*, 2020, **10**, 2000478.
112 Y. Lu, Q. Shen, Q. Yu, F. Zhang, G. Li and W. Zhang, *J. Phys. Chem. C*, 2016, **120**, 28712.
113 G. Chen, Y. Zhu, Y. Ying, Y. Yao, Z. Hu, D. Zu, Z. Lin, C. W. Pao, Y. C. Zhang, L. Li, Y. Zhu and H. Huang, *Matter*, 2024, **7**, 2265.